https://doi.org/10.5194/acp-2022-433
Preprint. Discussion started: 28 June 2022

Atmospheric Chemistry and Physics Discussions
Open Access
EGU

Supercooled liquid water clouds observed over Dome C, Antarctica: temperature sensitivity and surface radiation impact

Philippe Ricaud[1], Massimo Del Guasta[2], Angelo Lupi[3], Romain Roehrig[1], Eric Bazile[1], Pierre Durand[4], Jean-Luc Attié[4], Alessia Nicosia[3] and Paolo Grigioni[5]

[1]CNRM, Université de Toulouse, Météo-France, CNRS, Toulouse, France (philippe.ricaud@meteo.fr; romain.roehrig@meteo.fr; eric.bazile@meteo.fr)

[2]INO-CNR, Sesto Fiorentino, Italy (massimo.delguasta@ino.cnr.it)

[3]ISAC-CNR, Bologna, Italy (a.lupi@isac.cnr.it; a.nicosia@isac.cnr.it)

[4]Laboratoire d'Aérologie, Université de Toulouse, CNRS, UPS, Toulouse, France (pierre.durand@aero.obs-mip.fr; jean-luc.attie@aero.obs-mip.fr)

[5]ENEA, Roma, Italy (paolo.grigioni@enea.it)

Correspondence: philippe.ricaud@meteo.fr

https://doi.org/10.5194/acp-2022-433
Preprint. Discussion started: 28 June 2022

Abstract

Clouds affect the Earth climate with an impact that depends on the cloud nature (solid/ liquid water). Although the Antarctic climate is changing rapidly, cloud observations are sparse over Antarctica due to few ground stations and satellite observations. The Concordia station is located on the East Antarctic Plateau (75°S, 123°E, 3233 m above mean sea level), one of the driest and coldest places on Earth. We used observations of clouds, temperature, liquid water and surface radiation performed at Concordia during 4 austral summers (December 2018-2021) to analyse the link between liquid water and temperature and its impact on surface radiation in the presence of supercooled liquid water (liquid water for temperature less than 0°C) clouds (SLWCs). Our analysis shows that, within SLWCs, temperature logarithmically increases from -36.0°C to -16.0°C when liquid water path increases from 1.0 to 14.0 g m^{-2}, and SLWCs positively impact the net surface radiation, which logarithmically increases by 0.0 to 50.0 W m^{-2} when liquid water path increases from 1.7 to 3.0 g m^{-2}. We finally estimate that SLWCs have a great potential radiative impact over Antarctica whatever the season considered, up to 5.0 W m^{-2} over the Eastern Antarctic Plateau and up to 30 W m^{-2} over the Antarctic Peninsula in summer.

https://doi.org/10.5194/acp-2022-433
Preprint. Discussion started: 28 June 2022

Atmospheric Chemistry and Physics Discussions

1. Introduction

Antarctic clouds play an important role in the climate system by influencing the Earth's radiation balance, both directly at high southern latitudes and, indirectly, at the global level through complex teleconnections (Lubin et al., 1998). However, in Antarctica, ground stations are mainly located on the coast and yearlong observations of clouds and associated meteorological parameters are scarce. Meteorological analyses and satellite observations of clouds can nevertheless give some information on cloud properties suggesting that clouds vary geographically, with a fractional cloud cover ranging from about 50 to 60% around the South Pole to 80-90% near the coast (Bromwich et al., 2012; Listowski et al., 2019). In situ aircraft measurements performed mainly over the Western Antarctic Peninsula (Grosvenor et al., 2012; Lachlan-Cope et al., 2016) and nearby coastal areas (O'Shea et al., 2017) provided new insights to polar cloud modelling and highlighted sea-ice production of Cloud-Condensation Nuclei and Ice Nucleating Particles (see e.g. Legrand et al., 2016). Mixed-phase clouds (made of solid and liquid water) are preferably observed near the coast (Listowski et al., 2019) with larger ice crystals and water droplets (Lachlan-Cope, 2010; Lachlan-Cope et al., 2016; Grosvenor et al., 2012; O'Shea et al., 2017; Grazioli et al., 2017). Based on the raDAR/liDAR-MASK (DARDAR) spaceborne products (Listowski et al., 2019), it has been found that clouds are mainly constituted of ice above the continent whereas the abundance of Supercooled Liquid Water (SLW, the water staying in liquid phase below 0°C) clouds depends on temperature and liquid/ice fraction, decreases sharply poleward, and is two to three times lower over the Eastern Antarctic Plateau than over the Western Antarctic. An important point remains the inability of both research and operational weather prediction models to accurately represent the clouds (especially SLW clouds, SLWCs) in Antarctica causing biases of several tens W m^{-2} on net surface radiation (Listowski and Lachlan-Cope, 2017; King et al., 2006, 2015; Bromwich et al., 2013) over and beyond the Antarctic (Lawson and Gettelman, 2014; Young et al. 2019). From year-long LIDAR observations of mixed-phase clouds at South Pole (Lawson and Gettelman, 2014), SLWCs were shown to occur more frequently than in earlier aircraft observations or weather model simulations, leading to biases in the surface radiation budget estimates.

Liquid water in clouds may occur in supercooled form through heterogeneous nucleation due to a relative lack of ice nuclei for temperature greater than -39°C and less than 0°C. Very little SLW is then expected because the ice crystals that form in this temperature range will grow at the expense of liquid droplets (called the "Wegener-Bergeron-Findeisen" process; Storelvmo and Tan, 2015). Nevertheless, SLW is often observed at negative temperatures higher than -20°C at all latitudes being a danger to aircraft since icing on the wings and airframe can occur, reducing lift, and increasing drag and weight. As temperature decreases to -36°C, SLW dramatically lessens, so it is highly difficult 1) to observe SLWCs and 2) to quantify the amount of liquid water present in SLWCs. But during the Year Of Polar Prediction (YOPP) international campaign, recent observations performed at the Dome C station in Antarctica of 2 case studies in December 2018 have revealed SLWCs with temperature between -20°C and -30°C and Liquid Water Path (LWP, the liquid water concentration integrated along the vertical) between 2 to 20 g m^{-2}, as well as a considerable impact on the net Surface Radiation (SR) that exceeded the simulated values by 20-50 W m^{-2} (Ricaud et al., 2020).

The Dome C (Concordia) station, jointly operated by French and Italian institutions in the Eastern Antarctic Plateau (75°06'S, 123°21'E, 3233 m above mean sea level, amsl), is one of the driest and coldest places on Earth with surface temperatures ranging from about -20°C in summer to -70°C in winter. There are three main instruments relevant to this study that have been routinely running for about 10 years: 1) The H_2O Antarctica Microwave Stratospheric and Tropospheric Radiometer (HAMSTRAD, Ricaud et al., 2010a) to obtain vertical profiles of temperature and water vapour, as well as the LWP. 2) The tropospheric depolarization LIDAR (Tomasi et al., 2015) to obtain vertical profiles of backscatter and depolarization to be used for the detection of SLWCs. 3) The Baseline Surface Radiation Network (BSRN) station to measure surface longwave (4–50 µm) and shortwave (0.3–3 µm), downward and upward radiation from which the Net Surface Radiation (Net SR), calculated as the difference between the downward and upward SRs, can be computed (Driemel et al., 2018) as:

$$\text{Net SR} = \text{LWD SR} - \text{LWU SR} + \text{SWD SR} - \text{SWU SR} \tag{1}$$

where LWD SR, LWU SR, SWD SR and SWU SR correspond to Longwave Downward, Longwave Upward, Shortwave Downward and Shortwave Upward SRs, respectively.

The article is structured as follows. Section 2 presents the instruments during the period of study. In section 3, we detail the methodology employed to detect the SLWCs and calculate their impact on SR, and we present the statistical method to emphasize the relationship between temperature and LWP on one hand, and SR and LWP on the other hand. The results are highlighted in section 4 and discussed in section 5, before concluding in section 6.

2. Instruments

We have used the observations from 3 instruments held at the Dome C station, namely the LIDAR instrument to classify the cloud as SLWC, the HAMSTRAD microwave radiometer to obtain vertical profiles of temperature and Liquid Water Path (LWP) and the BSRN network to measure the Surface Radiation (SR) components: LWD, LWU, SWD and SWU to finally obtain the Net SR.

2.1. LIDAR

The tropospheric depolarization LIDAR (532 nm) has been operating at Dome C since 2008 (see http://lidarmax.altervista.org/englidar/_Antarctic%20LIDAR.php). The LIDAR provides 5-min tropospheric profiles of aerosols and clouds continuously, from 20 to 7000 m above ground level (agl), with a resolution of 7.5 m. LIDAR depolarization (Mishchenko et al., 2000) is a robust indicator of non-spherical shape for randomly oriented cloud particles. A depolarization ratio below 10% is characteristic of SLWC, while higher values are produced by ice particles. The possible ambiguity between SLWC and oriented ice plates is avoided at Dome C by operating the LIDAR 4° off-zenith (Hogan and Illingworth, 2003).

2.2. HAMSTRAD

HAMSTRAD is a microwave radiometer that profiles water vapour, liquid water and tropospheric temperature above Dome C. Measuring at both 60 GHz (oxygen molecule line (O_2) to deduce the temperature) and 183 GHz (H_2O line), this unique, state-of-the-art radiometer was installed on site for the first time in January 2009 (Ricaud et al., 2010a and b). The measurements of the HAMSTRAD radiometer allow the retrieval of the vertical profiles of water vapour and temperature from the ground to 10-km altitude with vertical resolutions of 30 to 50 m in the Planetary Boundary Layer (PBL), 100 m in the lower free troposphere and 500 m in the upper troposphere-lower stratosphere. The time resolution is adjustable and fixed at 60 seconds since 2018. Note that an automated internal calibration is performed every 12 atmospheric observations and lasts about 4 minutes. Consequently, the atmospheric time sampling is 60 seconds for a sequence of 12 profiles and a new sequence starts 4 minutes after the end of the previous one. The temporal resolution on the instrument allows for detection and analysis of atmospheric processes such as the diurnal evolution of the PBL (Ricaud et al., 2012) and the presence of clouds and diamond dust (Ricaud et al., 2017) together with SLWC (Ricaud et al., 2020). In addition, the LWP (g m^{-2}) that gives the amount of liquid water integrated along the vertical can also be estimated. Observations of LWP have been performed when the instrument was installed at the Pic du Midi station (2877 amsl, France) during the calibration/validation period in 2008 prior to its set up in Antarctica in 2009 (Ricaud et al., 2010a) and during the Year Of Polar Prediction (YOPP) campaign in summer 2018-2019 (Ricaud et al., 2020). At the present time, it has not yet been possible to compare HAMSTRAD LWP retrievals with observations from other instruments, neither at the Pic du Midi nor at

https://doi.org/10.5194/acp-2022-433
Preprint. Discussion started: 28 June 2022

Dome C stations. To better evaluate its performance, the 2021-2022 and the future 2022-2023 summer campaigns are dedicated to in-situ observations of SLWCs. Comparisons with numerical weather prediction models were showing consistent amounts of LWP at Dome C when the partition function between ice and liquid water was favouring SLW for temperatures less than 0°C (Ricaud et al., 2020).

2.3. BSRN

The BSRN sensors at Dome C are mounted at the Astroconcordia/Albedo-Rack sites, with upward and downward looking, heated and ventilated Kipp&Zonen CM22 pyranometers and CG4 pyrgeometers providing measurements of hemispheric downward and upward broadband shortwave (SW, 0.3–3 μm) and longwave (LW, 4–50 μm) fluxes at the surface, respectively. These data are used to retrieve values of net surface radiation. All these measurements follow the rules of acquisition, quality check and quality control of the BSRN (Driemel et al., 2018).

2.4. Period of study

From the climatological study presented in Ricaud et al. (2020), the SLWCs are mainly observed above Dome C in summer, with a higher occurrence in December than in January: 26% in December against 19% in January representing the percentage of days per month that SLW clouds were detected during the YOPP campaign (summer 2018-2019) within the LIDAR data for more than 12 hours per day. We have thus concentrated our analysis on December and the 4 years: 2018-2021. Since we have to use the three data sets (LIDAR, HAMSTRAD and BSRN) in time coincidence, the actual number of days per year selected in our analysis is presented in Table 1.

https://doi.org/10.5194/acp-2022-433
Preprint. Discussion started: 28 June 2022

3. Methodology

3.1. SLWC detection and Surface Radiation Impact

Consistent with Ricaud et al. (2020), we use LIDAR observations to discriminate between SLW and ice in a cloud. High values of LIDAR backscatter ($\beta > 100\ \beta_{mol}$, with β_{mol} the molecular backscatter) associated with very low depolarization ratio (< 5%) signifies the presence of a SLWC whilst high depolarization ratio (>20%) indicates the presence of an ice cloud or precipitation. Once the SLWC is detected both in time and altitude, the temperature (θ) profile within the cloud and the LWP measured by the HAMSTRAD radiometer in time coincidence are selected together with the SR observed by the BSRN instruments: Net, LWD, LWU, SWD and SWU SR. Figure 1 shows, as a typical example, the time evolution of the LIDAR backscatter and depolarization ratio, the HAMSTRAD LWP and temperature vertical profile for the 27 December 2021. Associated with these SLWCs, the LWP increases with time from 1.0 to 3.0 g m^{-2}. The SLWCs are present over a temperature range varying from about -28.0 °C to -33.0 °C. Note the cloud present at 04:00-05:00 UTC that is not labelled as a SLWC but rather as an ice cloud (high backscatter and high depolarization signals) with no associated increase of LWP and temperature above -28.0 °C.

Figure 2 highlights the time evolution of the SLWC obtained on 27 December 2021 together with some snapshots from the HALO-CAM video camera taken with or without SLWC on: 01:00 (no SLWC), 07:19 (SLWC), 09:00 (no SLWC), 10:14 (SLWC), 13:00 (no SLWC), 16:03 (SLWC), 18:01 (no SLWC) and 20:53 UTC (SLWC). SLWCs (high backscatter and low depolarization signals) are clearly detected at 07:00-08:00, 10:00-11:00, 16:00-17:00, 21:00-22:00 and 23:00-24:00 UTC over an altitude range 500-1000 m above ground level (agl). In general, SLWCs observed over the station did not correspond to overcast conditions.

Over the 4 summers (December 2018-2021), we have selected 3 datasets in time coincidence with SLWC: LWP, θ and SR. In order to estimate the impact of the SLWC onto

https://doi.org/10.5194/acp-2022-433
Preprint. Discussion started: 28 June 2022

the SR, we calculated the anomaly of the daily SR with respect to the clear-sky SR associated to the same day. Since it is impossible to measure for the same day the SR with and without cloud, we have considered, over the 4-summer period, clear-sky 24-hour periods. Only 5 clear-sky days were selected on: 2 and 19 December 2018, and 3, 17 and 26 December 2021. We have considered these 5 days as the reference SRs (SR_{Ref}) presented Figure 3. We have also calculated (Figure 4) the time evolution of the clear-sky surface radiation variability (δSR_{Ref}), namely the difference in SR observed by the BSRN instruments between each of 5 clear-sky day and the corresponding values averaged over the 5 days, for Net, LWD, LWU, SWD and SWU SR. The SR_{Ref} for the 5 days shown Figure 3 are all consistent to each other with an obvious diurnal cycle in Net, LWD, LWU, SWD and SWU SR (we recall that in December there is a 24-h solar illumination at Dome C). The variability within the 5 days (δSR_{Ref}) shown Figure 4 is within ±20 W m^{-2} for the Net SR with a greater Net SR in 2018 than in 2021, within ±35 W m^{-2} for LWD and LWU SR (maxima on 17 December 2021 and minima on 2 December 2018), and within ±25 W m^{-2} for SWD and SWU SR (maxima on 26 December 2021 and minima on 2 December 2018).

Based on these 5 SR_{Ref}, we performed a systematic study over the 4-summer period by calculating the surface radiation anomaly ΔSR defined as:

$$\Delta SR = SR - SR_{Ref} \quad (2)$$

for Net, LWD, LWU, SWD and SWU. As an example, we show in Figure 5 the time evolution for 27 December 2021 of the presence of the SLWC together with ΔSR calculated with respect to SR_{Ref} set to 26 December 2021. Associated with the SLWC, LWD and LWU ΔSR increase by 30-50 and 10-30 W m^{-2}, respectively, whilst SWD and SWU ΔSR decrease by 50-150 W m^{-2}, respectively. The effect on the Net ΔSR is positive (10-100 W m^{-2}) at 07:00-08:00, 10:00-11:00, 16:00-17:00 UTC and negative (from -30 to -100 W m^{-2}) at 21:00-22:00 and 23:00-24:00 UTC. We thus want to statistically analyse all the ΔSR calculated in 2018-2021 with the 5 SR_{Ref}

https://doi.org/10.5194/acp-2022-433
Preprint. Discussion started: 28 June 2022

in order to check whether the net effect of the SLWC on the SR is positive or negative and to evaluate its sensitivity to liquid water amounts.

3.2. Statistical Method

The datasets are binned into 1°C-wide bins for θ, 0.2 g m^{-2}-wide bins for LWP, and 5 W m^{-2}-wide bins for ΔSR. The number of points per bin is calculated for all the paired datasets, namely θ-LWP, and ΔSR-LWP (Net ΔSR-LWP, LWD ΔSR-LWP, LWU ΔSR-LWP, SWD ΔSR-LWP and SWU ΔSR-LWP). The 2D distribution of the Probability Density Function (PDF) is calculated for the paired datasets and defined as $PDF_{ij} = 100\,\frac{N_{ij}}{N_t}$, where N_{ij} and N_t are the count number in the bin *ij* and the total count number ($N_t = \sum_{j=1}^{N}\sum_{i=1}^{M} N_{ij}$), respectively, with *M* and *N* being the total number of bins in LWP on one side, and in temperature or ΔSR on the other side, respectively. For each value of θ_j within a 1°C-wide bin *j* or ΔSR_j within a 5 W m^{-2}-wide bin *j*, a weighted average of LWP ($\overline{LWP_j}$) is calculated together with its associated weighted standard deviation ($\sigma_{LWP\,j}$) considering all the LWP_{ij} values within 0.2 g m^{-2}-wide bins from *i*=1 to *M*, with *M* the total number of LWP bins and w_{ij} the weight, namely the number of points ($w_{ij} = N_{ij}$), associated to the bin *ij*:

$$\overline{LWP_j} = \frac{\sum_{i=1}^{M} w_{ij}\, LWP_{ij}}{\sum_{i=1}^{M} w_{ij}} \tag{3}$$

and

$$\sigma_{LWP\,j} = \sqrt{\frac{\sum_{i=1}^{M} w_{ij}\,(LWP_{ij} - \overline{LWP_j})^2}{\sum_{i=1}^{M} w_{ij}}} \tag{4}$$

For each θ and ΔSR dataset, the distribution of the total count numbers N_{tj} per 1°C or 5 W m^{-2}-wide bin ($N_{tj} = \sum_{i=1}^{M} N_{ij}$ with *j* = 1, …, *N*) can be fitted by a function $N(x)$, with *x* = θ or ΔSR, based on 2 to 3 Gaussian distributions as:

$$N(x) = \sum_{k=1}^{2\text{ or }3} a_k \exp\left(-\frac{1}{2}\left(\frac{x-\mu_k}{\sigma_k}\right)^2\right) + c \tag{5}$$

https://doi.org/10.5194/acp-2022-433
Preprint. Discussion started: 28 June 2022

with a_k, μ_k and σ_k being the amplitude, the mean and the standard deviation of the k^{th} Gaussian function (k = 1, 2 or 3) and c is a constant. We have used k = 2 for ΔSR and k = 3 for θ. Table 2 lists all the fitted parameters (a_k, μ_k, σ_k and c with k = 1 to 2 or 3).

In the relationship between x (θ or ΔSR) and LWP, we have considered x_j (θ_j or ΔSR_j) to be significant when:

$$x_j \leq \mu_k \pm \sigma_k \text{ for } k = 1 \text{ or } 2 \text{ (for } \Delta SR\text{) or } 3 \text{ (for } \theta\text{)} \tag{6}$$

and highlighted this significant point by showing the associated $\overline{LWP_j}$ and $\sigma_{LWP\,j}$ with j = 1, …, N.

Finally, a logarithmic function of the form

$$x = a + b\ln(\overline{LWP}) \tag{7}$$

has been fitted onto these significant points ($\overline{LWP_j} \pm \sigma_{LWP\,j}$, x_j) where the retrieved constants a and b are shown in Table 3 for x being θ, Net ΔSR, LWD ΔSR, LWU ΔSR, SWD ΔSR and SWU ΔSR.

4. Results

4.1. Temperature-Liquid Water Relationship in Supercooled Liquid Water Clouds

The relationship between temperature and LWP within SLWCs over the 4-summer period at Dome C is presented Figure 6 left in the form of a Probability Density Function (PDF) that is the fraction of points within each bin of 0.2 g m^{-2} width in LWP and 1.0°C width in temperature. It clearly shows a net tendency for liquid water to increase with temperature, up to ~14 g m^{-2} in LWP and -18°C in temperature, with two zones having a density as high as ~2%, at [0.5 g m^{-2}, -33°C] and [1.5 g m^{-2}, -32°C]. Performing a weighted average of the LWPs within each temperature bin (Figure 6 centre), fitting a Gaussian distribution of the count numbers as a function of temperature (Figure 6 right) and considering only temperature bins within one-sigma of the centre of the Gaussian distributions, we can fit the following

https://doi.org/10.5194/acp-2022-433
Preprint. Discussion started: 28 June 2022

logarithmic relation of the temperature θ as a function of LWP within the SLWC (Figure 6 centre):

$$\theta(LWP) = -33.8\ (\pm 1.5) + 6.5 \ln(LWP) \quad (8)$$

for $\theta \in [-36; -16]$ °C and $LWP \in [1.0; 14.0]$ g m^{-2}, where ($\pm$1.5) corresponds to the range where the relationship is valid within the 2 blue dashed lines in Figure 6 centre. In other words, based on our study, we have a clear evidence that supercooled liquid water exponentially increases with temperature. Although the amount of LWP is very low ($\ll$ 20 g m^{-2}) at Dome C compared to what can be measured and modelled (Lemus et al., 1997) in the Arctic (50-75 g m^{-2}) and at middle/tropical latitudes (100-150 g m^{-2}), we intended to estimate its impact on the SR at Dome C.

4.2. Impacts of Supercooled Liquid Water Clouds on Surface Radiation

In Figures 7 to 9, the left panel presents the PDF (for bins of 0.2 g m^{-2} width in LWP and 5 W m^{-2} width in ΔSR) of the surface radiation anomaly ΔSR as a function of the LWP, for Net, LWD, LWU, SWD and SWU, respectively. The central panel shows, for the same parameters, the corresponding weighted average LWP within 5 W m^{-2}-wide bins of radiation anomaly whereas the right panel shows the corresponding count number within 5 W m^{-2}-wide bins.

Based on our analysis, the relationship between Net ΔSR (in W m^{-2}) and the LWP (in g m^{-2}) has been estimated from the HAMSTRAD and BSRN data as:

$$Net\ \Delta SR(LWP) = -50.0\ (\pm 10.0)\ + 90.0 \ln(LWP) \quad (9)$$

for $Net\ \Delta SR \in [-15; 50]$ W m^{-2} and $LWP \in [1.5; 3.0]$ g m^{-2}, where ($\pm$10.0) corresponds to the range where the relationship is valid within the 2 blue dashed lines in Figure 7 centre. Thus, for LWP greater than 1.7 g m^{-2}, our study clearly shows that there is a positive impact of SLWC on the Net ΔSR that can reach 50 W m^{-2} for an LWP of 3.0 g m^{-2}.

The splitting of the net radiation anomaly between each of its four components can be evaluated from their individual relationships with the LWP. These relations are gathered in

Table 3, established from the plots presented in Figures 7 to 9. They are of the same form as for net surface radiation anomaly, i.e. a logarithmic dependence on LWP. Table 3 presents the coefficients *a* and *b* of the logarithmic function $f(LWP) = a + b\ln(LWP)$ for the temperature θ or the radiation components ΔSR, together with the valid range of these relations for $\theta, \Delta SR$ and LWP. For the values presented in Table 3, our study clearly shows that SLWCs have a positive impact on LWD and LWU, with ΔSR increasing from 0 to 100 W m^{-2} and from 0 to 40 W m^{-2} for LWP ranging from 1.0 to 4.0 and from 1.6 to 2.5 g m^{-2}, respectively.

Furthermore, our study also shows that SLWCs have a clear negative impact on SWD and SWU, with ΔSR decreasing from 0 to -140 W m^{-2} and from 0 to -75 W m^{-2} with LWP ranging from 1.2 to 3.8 and from 1.2 to 3.2 g m^{-2}, respectively.

5. Discussion

5.1. Logarithmic Dependency

It is interesting to note that the relationships we have obtained in our study showing an exponential dependence of LWP on both temperature and SR anomaly is very similar to the dependence of the molar volume and density of water on critical temperature. As a matter of fact, the density ρ (g cm^{-3}) and molar volume ν (cm^{3} mol^{-1}) of liquid water are exponentially varying with temperature (Sippola and Taskinen, 2018):

$$\rho = \rho_0 \exp\{-T_c(A + B\varepsilon + 2C\varepsilon^{1/2})\} \quad (10)$$

$$\nu = \frac{M_{H_2O}}{\rho} = \frac{M_{H_2O}}{\rho_0} \exp\{T_c(A + B\varepsilon + 2C\varepsilon^{1/2})\} \quad (11)$$

where ρ_0 (g cm^{-3}), A (K^{-1}), B (K^{-1}), and C (K^{-1}) are parameters; T_c is the critical temperature whose value varies from 227 to 228 K, and M_{H_2O} (g mol^{-1}) is the molecular weight of water. ε (unitless) is defined as:

$$\varepsilon = \frac{T}{T_c} - 1 \quad (12)$$

https://doi.org/10.5194/acp-2022-433
Preprint. Discussion started: 28 June 2022

where T is temperature in K.

5.2. Modelling SLWC

Previous studies have already underlined the difficulty to model the SLWC together with its impact on surface radiations. Modelling SLWCs over Antarctica is challenging because 1) operational observations from meteorological radiosondes are scarce since the majority of ground stations are located at the coast and very few of them are maintained all year long, and satellite observations are limited to 60°S in geostationary orbit whilst, in polar orbit, the number of available orbits does not exceed 15 per day, and 2) the model should provide a partition function favouring liquid water at the expense of ice for temperatures between -36°C and 0°C in order to calculate realistic SLW concentrations. Differences of 20 to 50 W m^{-2} in the Net SR were found in the Arpege model (Pailleux et al., 2015) between clouds made of ice or liquid water during the summer 2018-2019 (Ricaud et al., 2020), differences that are very consistent with the results obtained in the present study. Although SLWCs are less present over the Antarctic Plateau than over the coastal region, their radiative impact is not negligible and should be taken into account with great care in order to estimate the radiative budget of the Antarctic continent in one hand, and, on the other hand, over the entire Earth.

5.3. Errors

Measurements of temperature, LWP, depolarization signal and SR are altered by random and systematic errors that may affect the relationships we have obtained between LWP and either temperature or SR anomalies. The temperature measured by HAMSTRAD below 1 km has been evaluated against radiosonde coincident observations from 2009 to 2014 (Ricaud et al., 2015) and the resulting bias is 0-2°C below 100 m and between -2 and 0°C between 100 and 1000 m. SLWCs are usually located around 400-600 m above the ground where the cold bias can be estimated to be about -1.0°C. The one-sigma (1-σ) root mean square (RMS) temperature error over a 7-min integration time is 0.25°C in the PBL and 0.5°C in the free

https://doi.org/10.5194/acp-2022-433
Preprint. Discussion started: 28 June 2022

troposphere (Ricaud et al., 2015). As a consequence, given the number of points used in the statistical analysis (>1000), the random error on the weighted-average temperature is negligible (<0.02°C). The LWP random and systematic errors are difficult to evaluate since there is no coincident external data to compare with. Nevertheless, the 1-σ RMS error over a 7-min integration time can be estimated to be 0.25 g m^{-2} giving a random error on the weighted average LWP less than 0.08 g m^{-2}. Based on clear-sky observations, the positive bias can be estimated to be less than 0.4 g m^{-2}. Theoretically, SLW should not exist at temperatures less than -39°C although it has been observed in recent laboratory measurements down to -42.55°C (Goy et al., 2018). Using equation (8) with an LWP bias of 0.4 g m^{-2} gives a temperature of -39.8°C (~0.8°C lower than the theoretical limit of -39°C), so the biases estimated for temperature and LWP are very consistent with theory.

The estimation of systematic and random errors on LIDAR backscattering and depolarization signals and their impact on the attribution/selection of SLWC is not trivial. But the most important point is to evaluate whether the observed cloud is constituted of purely liquid or mixed-phase water. Even considering the backscatter intensity only, we could not exclude that ice particles could have been present in the SLWC events investigated in 2018 (Ricaud et al., 2020). Therefore, in the present analysis, although we made a great attention to diagnose ice in the LIDAR cloud observations, we cannot totally exclude ice particles thus mixed-phase parcels were actually present when we labelled the observed cloud as SLWCs.

The 4 instruments providing LWD, LWU, SWD and SWU SR follow the rules of acquisition, quality check and quality control of the BSRN (Driemel et al., 2018). In polar regions (Lanconelli et al., 2011), the global SWU and SWD SRs are expected to be affected by random errors up to ±20 W m^{-2} while LWD SRs are expected to be affected by random errors not greater than ±10 W m^{-2} (Ohmura et al., 1998). As a consequence, given the large number of observations used per 5 W m^{-2}-wide bins (1000-3000), the random error on the weighted-average SRs is negligible (0.3-0.7 W m^{-2}) whatever the radiations considered, LW and SW.

Finally, apart from the instrument-related SR_{Ref} error, another source of error comes from 1) the geometry of observation and 2) the discontinuous SLWC layer. Firstly, LIDAR is almost zenith pointing, HAMSTRAD makes a scan in the East direction (from 10° elevation to zenith), whilst the BSRN radiometers detect the radiation in a 2π-steradians field of view (3D configuration). That is to say, in our analysis, the whole sky contributes to the radiation whilst only the cloud at zenith (1D configuration) and on the East direction (2D configuration) is observed by the LIDAR and HAMSTRAD, respectively. Secondly, SLWCs cannot be considered as uniform in the whole (see e.g. broken cloud fields in Figure 2).

5.4. Other clouds

Although the method we have developed to select the SLWCs has been validated using the amount of LWP and, in another study, using space-borne observations (Ricaud et al., 2020), we cannot rule out that, associated with the SLW droplets, are also ice particles, that is clouds are constituted of a mixture of liquid and solid water. Generally, such clouds are a superposition of a lower layer being made of liquid water and an upper layer being made of solid water (see Fig. 12.3 from Lamb and Verlinde, 2011). These mixed-layer clouds do not significantly modify the relationship between temperature and LWP because 1) SLW observations from HAMSTRAD are only sensitive to water in liquid phase and 2) temperature from HAMSTRAD is selected at times and vertical heights where the LIDAR depolarization signal is very low (<5%). Although we have verified that pure ice clouds were not selected by our method, we cannot differentiate mixed-phase clouds from purely SLWCs. As a consequence, the relationship between ΔSR and LWP might be affected by the presence of mixed-phased clouds in addition to SLWCs. This may explain the negative part of the Net, LWD and LWU ΔSR ($[-20; 0]$ W m^{-2}) and the

https://doi.org/10.5194/acp-2022-433
Preprint. Discussion started: 28 June 2022

positive part of the SWD and SWU ΔSR ([0; 10] W m^{-2}) for low values of LWP ([0.8; 1.6] g m^{-2}).

Furthermore, we already have noticed that SLWCs developed at the top of the PBL (Ricaud et al., 2020) in the "entrainment zone" and maintained in the "capping inversion zone", following the terminology of Stull (2012), at a height ranging from 100 to 1000 m above ground level. Nevertheless, during the local "night" at 00:00-06:00 LT, the PBL may collapse down to a very low height ranging 20-50 m. In this configuration, it is hard to differentiate from LIDAR observations between a SLWC and a fog episode, although the LIDAR can measure depolarization (but not backscatter) down to approximately 10-30 m above the ground (Figure S3 in Chen et al., 2017), so that we can distinguish liquid/frozen clouds very close to the ground.

Finally, we cannot rule out that, above the SLWCs that are actually observed by both LIDAR and HAMSTRAD, other clouds might be present, as e.g. cirrus clouds constituted of ice crystals. These mid-to-upper tropospheric clouds cannot be detected by HAMSTRAD (no sensitivity to ice crystals). In the presence of SLWCs either low in altitude or optically thick, the LIDAR backscatter signal is decreased in order to avoid saturation and the signal from upper layers is thus almost cancelled. These mid-to-high-altitude clouds are observed by the BSRN instruments and SR can be affected in this configuration. Based on the presence of cirrus clouds before or after the SLWCs (and sometimes during the SLWCs if optically thin), we can estimate that the number of days when SLWCs and cirrus clouds are simultaneously present to cover less than 10% of our period of interest.

5.5. Potential radiative impact of SLWCs over Antarctica

Based on our results and on the observed cloud fraction (η_{CF}) of SLWCs over Antarctica for different seasons (Listowski et al., 2019), we have estimated the potential radiative impact of SLWCs at the scale of the Antarctic continent ($Net\ \Delta SR^{max}_{global}$) from the maximum of $Net\ \Delta SR$ ($Net\ \Delta SR^{max} = 50$ W m^{-2}) computed in our study:

https://doi.org/10.5194/acp-2022-433
Preprint. Discussion started: 28 June 2022

$$Net\ \Delta SR_{global}^{max} = \eta_{CF} \times Net\ \Delta SR^{max} \quad (13)$$

In December, if we consider η_{CF} for SLW-containing cloud that is to say both mixed-phase cloud and unglaciated SLW cloud consistent with our study, we find for a lower-level altitude cut-off of 0, 500 and 1000 m (Figure B1 in Listowski et al., 2019), a potential radiative impact $Net\ \Delta SR_{global}^{max}$ over Antarctica of 9, 7 and 5 W m^{-2}, respectively. We now separate the Eastern elevated Antarctic Plateau from the Western Antarctica (Figure 5 in Listowski et al., 2019) for the 4 seasons. Over Eastern Antarctica, we find that $Net\ \Delta SR_{global}^{max} =$ 0.5-5.0 W m^{-2} in December-January-February (DJF) and 0-2.5 W m^{-2} for the remaining seasons. Over Western Antarctica, the potential radiative impact is much more intense because of higher temperatures and lower elevations compared to the Eastern Antarctic Plateau: $Net\ \Delta SR_{global}^{max} =$ 12.5-30.0 W m^{-2} in DJF (30 W m^{-2} over the Antarctica Peninsula); 7.5-20.0 W m^{-2} in March-April-May; 2.5-10.0 W m^{-2} in June-July-August; and 5.0-12.5 W m^{-2} in September-October-November.

6. Conclusions

Combining the observations of temperature, water vapour and liquid water path from a ground-based microwave radiometer, backscattering and depolarization from a ground-based LIDAR and surface radiations at long and short wavelengths, our analysis has been able to evaluate the presence of supercooled liquid water clouds over the Dome C station in summer. Focussing on 4 Decembers (2018-2021), the sensitivity of the SLWCs to temperature and LWP has been established with temperature logarithmically increasing from -36.0°C to -16.0°C when liquid water path increases from 1.0 to 14.0 g m^{-2}. We have also evaluated that SLWCs positively affect the net surface radiation, which logarithmically increases from 0.0 to 50.0 W m^{-2} when liquid water path increases from 1.7 to 3.0 g m^{-2}. Our study clearly shows that: 1) SLWCs have a positive impact on LWD and LWU, with ΔSR increasing from 0 to 100 W m^{-2} and from 0 to 40 W m^{-2} for LWP ranging from 1.0 to 4.0 and from 1.6 to 2.5 g m^{-2}, respectively,

https://doi.org/10.5194/acp-2022-433
Preprint. Discussion started: 28 June 2022

and 2) SLWCs have a clear negative impact on SWD and SWU, with ΔSR decreasing from 0 to -140 W m^{-2} and from 0 to -75 W m^{-2} with LWP ranging from 1.2 to 3.8 and from 1.2 to 3.2 g m^{-2}, respectively.

Finally, extrapolating the radiative impact of the SLWCs from the Dome C station to the Antarctic continent shows that SLWCs have a great potential radiative impact all over Antarctica whatever the season considered, up to 5.0 W m^{-2} over the Eastern Antarctic Plateau and up to 30 W m^{-2} over the Antarctic Peninsula in DJF. This stresses the importance of accurately modelling SLWCs when calculating the Earth energy budget to adequately forecast the Earth climate evolution, especially since the climate is rapidly changing in Antarctica, as illustrated by the surface temperature record of -12°C recently observed in March 2022 at the Concordia station and largely publicized worldwide (see e.g. https://www.latimes.com/world-nation/story/2022-03-19/antarctica-and-arctic-70-and-50-degrees-above-normal).

Data availability

HAMSTRAD data are available at http://www.cnrm.meteo.fr/spip.php?article961&lang=en (last access: 3 May 2022). The tropospheric depolarization LIDAR data are reachable at http://lidarmax.altervista.org/lidar/home.php (last access: 3 May 2022). Radiosondes are available at http://www.climantartide.it (last access: 3 May 2022). BSRN data can be obtained from the ftp server (https://bsrn.awi.de/data/data-retrieval-via-ftp/) (last access: 3 May 2022).

Author contribution

PR, MDG, and AL provided the observational data. PR developed the methodology. All the co-authors participated in the data analysis and in the data interpretation. PR prepared the manuscript with contributions from all co-authors.

Competing interests

The authors declare that they have no conflict of interest.

Acknowledgments

The present research project Water Budget over Dome C (H2O-DC) has been approved by the Year of Polar Prediction (YOPP) international committee. The HAMSTRAD programme (910) was supported by the French Polar Institute, Institut polaire français Paul-Emile Victor (IPEV), the Institut National des Sciences de l'Univers (INSU)/Centre National de la Recherche Scientifique (CNRS), Météo-France and the Centre National d'Etudes Spatiales (CNES). The permanently manned Concordia station is jointly operated by IPEV and the Italian Programma Nazionale Ricerche in Antartide (PNRA). The tropospheric LIDAR operates at Dome C from 2008 within the framework of several Italian national (PNRA) projects. We would like to thank all the winterover personnel who worked at Dome C on the different projects: HAMSTRAD, aerosol LIDAR and BSRN.

References

Bromwich, D. H., Nicolas, J. P., Hines, K. M., Kay, J. E., Key, E. L., Lazzara, Lubin, D., McFarquhar, G. M., Gorodetskaya, I. V., Grosvenor, D. P., Lachlan-Cope, T., and van Lipzig, N. P. M.: Tropospheric clouds in Antarctica, Rev. Geophys., 50, RG1004, https://doi.org/10.1029/2011RG000363, 2012.

Bromwich, D. H., Otieno, F. O., Hines, K. M., Manning, K. W., and Shilo, E.: Comprehensive evaluation of polar weather research and forecasting model performance in the Antarctic, J. Geophys. Res.-Atmos., 118, 274–292, 2013.

Chen, X., Virkkula, A., Kerminen, V.-M., Manninen, H. E., Busetto, M., Lanconelli, C., Lupi, A., Vitale, V., Del Guasta, M., Grigioni, P., Väänänen, R., Duplissy, E.-M., Petäjä, T., and

https://doi.org/10.5194/acp-2022-433
Preprint. Discussion started: 28 June 2022

Atmospheric Chemistry and Physics Discussions

Kulmala, M.: Features in air ions measured by an air ion spectrometer (AIS) at Dome C, Atmos. Chem. Phys., 17, 13783–13800, https://doi.org/10.5194/acp-17-13783-2017, 2017.

Driemel, A., Augustine, J., Behrens, K., Colle, S., Cox, C., Cuevas-Agulló, E., Denn, F. M., Duprat, T., Fukuda, M., Grobe, H., Haeffelin, M., Hodges, G., Hyett, N., Ijima, O., Kallis, A., Knap, W., Kustov, V., Long, C. N., Longenecker, D., Lupi, A., Maturilli, M., Mimouni, M., Ntsangwane, L., Ogihara, H., Olano, X., Olefs, M., Omori, M., Passamani, L., Pereira, E. B., Schmithüsen, H., Schumacher, S., Sieger, R., Tamlyn, J., Vogt, R., Vuilleumier, L., Xia, X., Ohmura, A., and König-Langlo, G.: Baseline Surface Radiation Network (BSRN): structure and data description (1992–2017), Earth Syst. Sci. Data, 10, 1491–1501, https://doi.org/10.5194/essd-10-1491-2018, 2018.

Goy, C., Potenza, M. A., Dedera, S., Tomut, M., Guillerm, E., Kalinin, A., Voss, K.-O., Schottelius, A., Petridis, N., Prosvetov, A., Tejeda, G., Fernández, J. M., Trautmann, C., Caupin, F., Glasmacher, U., and Grisenti, R. E.: Shrinking of rapidly evaporating water microdroplets reveals their extreme supercooling, Phys. Rev. Lett., 120, 015501, https://doi.org/10.1103/PhysRevLett.120.015501, 2018.

Grazioli, J., Genthon, C., Boudevillain, B., Duran-Alarcon, C., Del Guasta, M., Madeleine, J.-B., and Berne, A.: Measurements of precipitation in Dumont d'Urville, Adélie Land, East Antarctica, The Cryosphere, 11, 1797–1811, https://doi.org/10.5194/tc-11-1797-2017, 2017.

Grosvenor, D. P., Choularton, T. W., Lachlan-Cope, T., Gallagher, M. W., Crosier, J., Bower, K. N., Ladkin, R. S., and Dorsey, J. R.: In-situ aircraft observations of ice concentrations within clouds over the Antarctic Peninsula and Larsen Ice Shelf, Atmos. Chem. Phys., 12, 11275–11294, https://doi.org/10.5194/acp-12-11275-2012, 2012.

https://doi.org/10.5194/acp-2022-433
Preprint. Discussion started: 28 June 2022

Atmospheric Chemistry and Physics Discussions

Hogan, R. J. and Illingworth, A. J.: The effect of specular reflection on spaceborne lidar measurements of ice clouds, Report of the ESA Retrieval algorithm for EarthCARE project, 5 pp., 2003.

King, J. C., Argentini, S. A., and Anderson, P. S.: Contrasts between the summertime surface energy balance and boundary layer structure at Dome C and Halley stations, Antarctica, J. Geophys. Res.-Atmos., 111, D02105, https://doi.org/10.1029/2005JD006130, 2006.

King, J. C., Gadian, A., Kirchgaessner, A., Kuipers Munneke, P., Lachlan-Cope, T. A., Orr, A., Reijmer, C., Broeke, M. R., van Wessem, J. M., and Weeks, M.: Validation of the summertime surface energy budget of Larsen C Ice Shelf (Antarctica) as represented in three high-resolution atmospheric models, J. Geophys. Res.-Atmos., 120, 1335–1347, https://doi.org/10.1002/2014JD022604, 2015.

Lachlan-Cope, T.: Antarctic clouds, Polar Res., 29, 150–158, 2010.

Lachlan-Cope, T., Listowski, C., and O'Shea, S.: The microphysics of clouds over the Antarctic Peninsula – Part 1: Observations, Atmos. Chem. Phys., 16, 15605–15617, https://doi.org/10.5194/acp-16-15605-2016, 2016.

Lamb, D., and J. Verlinde: Physics and chemistry of clouds. Cambridge University Press, 2011.

Lanconelli, C., Busetto, M., Dutton, E. G., König-Langlo, G., Maturilli, M., Sieger, R., Vitale, V., and Yamanouchi, T.: Polar baseline surface radiation measurements during the International Polar Year 2007–2009, Earth Syst. Sci. Data, 3, 1–8, https://doi.org/10.5194/essd-3-1-2011, 2011.

Lawson, R. P. and Gettelman, A.: Impact of Antarctic mixed-phase clouds on climate, P. Natl. Acad. Sci. USA, 111, 18156–18161, 2014.

Legrand, M., Yang, X., Preunkert, S., and Therys, N.: Year-round records of sea salt, gaseous, and particulate inorganic bromine in the atmospheric boundary layer at coastal (Dumont d'Urville) and central (Concordia) East Antarctic sites, J. Geophys. Res. Atmos., 121, 997–1023, https://doi.org/10.1002/2015JD024066, 2016.

Lemus, L., Rikus, L., Martin, C., and Platt, R.: Global cloud liquid water path simulations. J. Climate, 10(1), 52-64, 1997.

Listowski, C. and Lachlan-Cope, T.: The microphysics of clouds over the Antarctic Peninsula – Part 2: modelling aspects within Polar WRF, Atmos. Chem. Phys., 17, 10195–10221, https://doi.org/10.5194/acp-17-10195-2017, 2017.

Listowski, C., Delanoë, J., Kirchgaessner, A., Lachlan-Cope, T., and King, J.: Antarctic clouds, supercooled liquid water and mixed phase, investigated with DARDAR: geographical and seasonal variations, Atmos. Chem. Phys., 19, 6771–6808, https://doi.org/10.5194/acp-19-6771-2019, 2019.

Lubin, D., Chen, B., Bromwich, D. H., Somerville, R. C., Lee, W. H., and Hines, K. M.: The Impact of Antarctic Cloud Radiative Properties on a GCM Climate Simulation, J. Climate, 11, 447-462, 1998.

Mishchenko, M. I., Hovenier, J. W., and Travis, L. D. (Eds.): Light Scattering by Nonspherical Particles: Theory, Measurements, and Applications, Academic Press, chap. 14, 393–416, 2000.

Ohmura, A., Dutton,E. G., Forgan, B., Fröhlich, C., Gilgen, H., Hegner, H., Heimo, A., König-Langlo, G., McArthur, B., Müller, G., Philipona, R., Pinker, R., Whitlock, C. H., Dehne, K., and Wild, M.: Baseline Surface Radiation Network (BSRN/WCRP): New precision radiometry for climate research, B. Am. Meteorol. Soc., 79(10), 2115-2136, 1998.

O'Shea, S. J., Choularton, T. W., Flynn, M., Bower, K. N., Gallagher, M., Crosier, J., Williams, P., Crawford, I., Flem- ing, Z. L., Listowski, C., Kirchgaessner, A., Ladkin, R. S., and Lachlan-Cope, T.: In situ measurements of cloud microphysics and aerosol over coastal

https://doi.org/10.5194/acp-2022-433
Preprint. Discussion started: 28 June 2022

Antarctica during the MAC campaign, Atmos. Chem. Phys., 17, 13049–13070, https://doi.org/10.5194/acp-17-13049-2017, 2017.

Pailleux, J., Geleyn, J.-F., El Khatib, R., Fischer, C., Hamrud, M., Thépaut, J.-N., Rabier, F., Andersson, E., Salmond, D., Burridge, D., Simmons, A., and Courtier, P.: Les 25 ans du système de prévision numérique du temps IFS/Arpège, La Météorologie, 89, 18–27, https://doi.org/10.4267/2042/56594, 2015.

Ricaud, P., Gabard, B., Derrien, S., Chaboureau, J.-P., Rose, T., Mombauer, A. and Czekala, H.: HAMSTRAD-Tropo, A 183-GHz Radiometer Dedicated to Sound Tropospheric Water Vapor Over Concordia Station, Antarctica, IEEE T. Geosci. Remote, 48, 1365–1380, doi: 10.1109/TGRS.2009.2029345, 2010a.

Ricaud, P., Gabard, B., Derrien, S., Attié, J.-L., Rose, T., and Czekala, H.: Validation of tropospheric water vapor as measured by the 183-GHz HAMSTRAD Radiometer over the Pyrenees Mountains, France, IEEE T. Geosci. Remote, 48, 2189–2203, 2010b.

Ricaud, P., Genthon, C., Durand, P., Attié, J.-L., Carminati, F., Canut, G., Vanacker, J.-F., Moggio, L., Courcoux, Y., Pellegrini, A., and Rose, T.: Summer to Winter Diurnal Variabilities of Temperature and Water Vapor in the lowermost troposphere as observed by the HAMSTRAD Radiometer over Dome C, Antarctica, Bound.-Lay. Meteorol., 143, 227–259, doi:10.1007/s10546-011-9673-6, 2012.

Ricaud, P., Grigioni, P., Zbinden, R., Attié, J.-L., Genoni, L., Galeandro, A., Moggio, A., Montaguti, S., Petenko, I., and Legovini, P.: Review of tropospheric temperature, absolute humidity and integrated water vapour from the HAMSTRAD radiometer installed at Dome C, Antarctica, 2009–14, Antarct. Sci., 27, 598-616, doi:10.1017/S0954102015000334, 2015.

Ricaud, P., Bazile, E., del Guasta, M., Lanconelli, C., Grigioni, P., and Mahjoub, A.: Genesis of diamond dust, ice fog and thick cloud episodes observed and modelled above Dome C,

https://doi.org/10.5194/acp-2022-433
Preprint. Discussion started: 28 June 2022

Antarctica, Atmos. Chem. Phys., 17, 5221-5237, https://doi.org/10.5194/acp-17-5221-2017, 2017.

Ricaud, P., Del Guasta, M., Bazile, E., Azouz, N., Lupi, A., Durand, P., Attié, J.-L., Veron, D., Guidard, V., and Grigioni, P.: Supercooled liquid water cloud observed, analysed, and modelled at the top of the planetary boundary layer above Dome C, Antarctica, Atmos. Chem. Phys., 20, 4167–4191, https://doi.org/10.5194/acp-20-4167-2020, 2020.

Sippola, H., and Taskinen, P.: Activity of supercooled water on the ice curve and other thermodynamic properties of liquid water up to the boiling point at standard pressure, J. Chem. Engineer. Data, 63(8), 2986-2998, 2018.

Storelvmo, T. and Tan, I.: The Wegener–Bergeron–Findeisen process—Its discovery and vital importance for weather and climate, Meteor. Z, 24, 455-461, 2015.

Stull, R. B.: An introduction to boundary layer meteorology, Vol. 13, Springer Science & Business Media, 2012.

Tomasi, C., Petkov, B., Mazzola, M., Ritter, C., di Sarra, A., di Iorio, T., and del Guasta, M.: Seasonal variations of the relative optical air mass function for background aerosol and thin cirrus clouds at Arctic and Antarctic sites, Remote Sensing, 7(6), 7157-7180, 2015.

Young, G., Lachlan-Cope, T., O'Shea, S. J., Dearden, C., Listowski, C., Bower, K. N., Choularton, T. W., and Gallagher, M. W.: Radiative effects of secondary ice enhancement in coastal Antarctic clouds, Geophys. Res. Lett., 46, 2312–2321, https://doi.org/10.1029/2018GL080551, 2019.

https://doi.org/10.5194/acp-2022-433
Preprint. Discussion started: 28 June 2022

Atmospheric Chemistry and Physics Discussions

Tables

Table 1. Time-coincident data availability (green) in Decembers 2018-2021 for HAMSTRAD temperature and LWP, Lidar Backscattering and Depolarization and BSRN Surface Radiances (Net, LWD, LWU, SWD and SWU). The 5 clear-sky (Reference) days are highlighted in red.

Year	December Days																													
	1	2	3	4	5	6	7	8	9	10	11	12	13	14	15	16	17	18	19	20	21	22	23	24	25	26	27	28	29	30	31
2018																															
2019																															
2020																															
2021																															

https://doi.org/10.5194/acp-2022-433
Preprint. Discussion started: 28 June 2022

Atmospheric Chemistry and Physics Discussions
Open Access
EGU

607

608 **Table 2.** Gaussian functions fitted to the $N(x)$ function for $x = \theta$ (°C) or ΔSR (W m^{-2}). Units
609 of a_1, a_2, a_3, and c are in count number for θ and ΔSR; units of μ_1, μ_2, μ_3, σ_1, σ_2, and σ_3 are
610 in °C for θ and in W m^{-2} for ΔSR.

x	a_1	μ_1	σ_1	a_2	μ_2	σ_2	a_3	μ_3	σ_3	c
$\boldsymbol{\theta}$	15.0 10^3	-31.5	1.45	5.0 10^3	-28.0	1.65	0.5 10^3	-19.0	2.5	-9.1 10^{-6}
Net ΔSR	2106.5	0.02	19.2	941.4	29.8	22.0	-	-	-	19.5
LWD ΔSR	1010.8	80.1	21.9	1565.6	10.0	23.9	-	-	-	18.4
LWU ΔSR	1476.4	-10.0	14.9	1834.7	25.0	16.2	-	-	-	185.4
SWD ΔSR	1317.2	-5.0	15.8	717.4	-80.0	64.7	-	-	-	9.1
SWU ΔSR	1928.8	-5.0	19.2	1163.4	-59.9	17.6	-	-	-	9.1

611

612

https://doi.org/10.5194/acp-2022-433
Preprint. Discussion started: 28 June 2022

Atmospheric Chemistry and Physics
Discussions
Open Access

Table 3. Coefficients of the relations $f(LWP) = a + b\ln(LWP)$ for the temperature θ or surface radiation anomalies ΔSR. Units of θ and ΔSR, as well as of their corresponding "a" values are in °C and W m^{-2}, respectively; units of b are in °C g^{-1} m^{2} for θ and in W / g for ΔSR; units of LWP are in g m^{-2}. The last column shows the range of LWP values for which the relation is valid (in black), and in red (blue) the sub-range in which a positive (negative) impact is observed on ΔSR. Note that $a \pm \delta a$ corresponds to the range of a values where the relationship is valid.

$f(LWP)$	$a \pm \delta a$	b	Valid range for θ or ΔSR	Valid range for LWP
θ	-33.8 $\pm$ 1.5	6.5	$[-36; -16]$	[1.0; 14.0]
Net ΔSR	-50.0 $\pm$ 10.0	90.0	$[-15; 50]$	[1.5; 3.0] / [1.7; 3.0]
LWD ΔSR	5.0 $\pm$ 15.0	65.0	$[-10; 100]$	[0.8; 4.0]/ [1.0; 4.0]
LWU ΔSR	-45.0 $\pm$ 30.0	90.0	$[-20; 40]$	[1.3; 2.5]/ [1.6; 2.5]
SWD ΔSR	30.0 $\pm$ 30.0	-130.0	$[-140; 10]$	[1.1; 3.8]/ [1.2; 3.8]
SWU ΔSR	15.0 $\pm$ 15.0	-75.0	$[-75; 10]$	[1.1; 3.2]/ [1.2; 3.2]

Figures

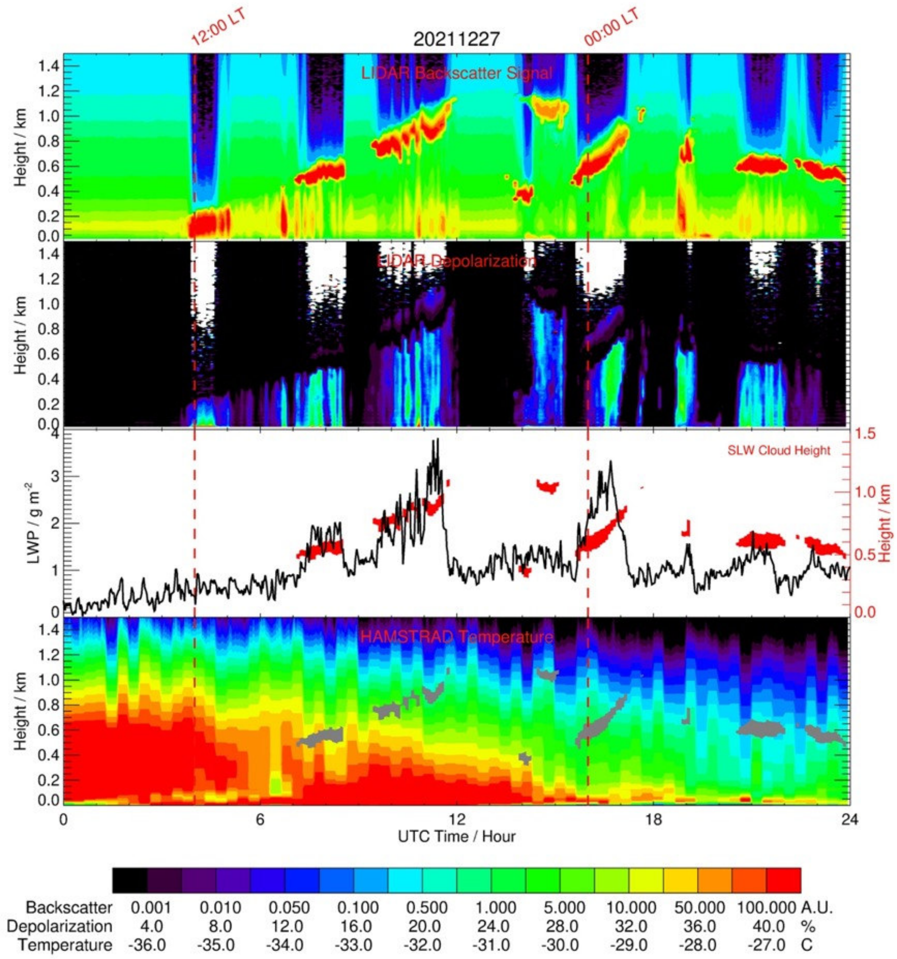

Figure 1: (From top to bottom): Time evolution (UTC, hour) of the Lidar Backscattering Signal, the Lidar Depolarization Signal, the HAMSTRAD LWP and the HAMSTRAD temperature profile measured on 27 December 2021. The time evolution of the SLW cloud (as diagnosed by a backscattering signal > 60 A.U. and a depolarization signal < 5%) is highlighted by the red and grey areas in the third and the forth panel from the top, respectively. The height above the ground is shown on the third panel from the top with the y-axis on the right. The 00:00 and 12:00 local times (LT) are highlighted by 2 vertical dashed lines.

https://doi.org/10.5194/acp-2022-433
Preprint. Discussion started: 28 June 2022

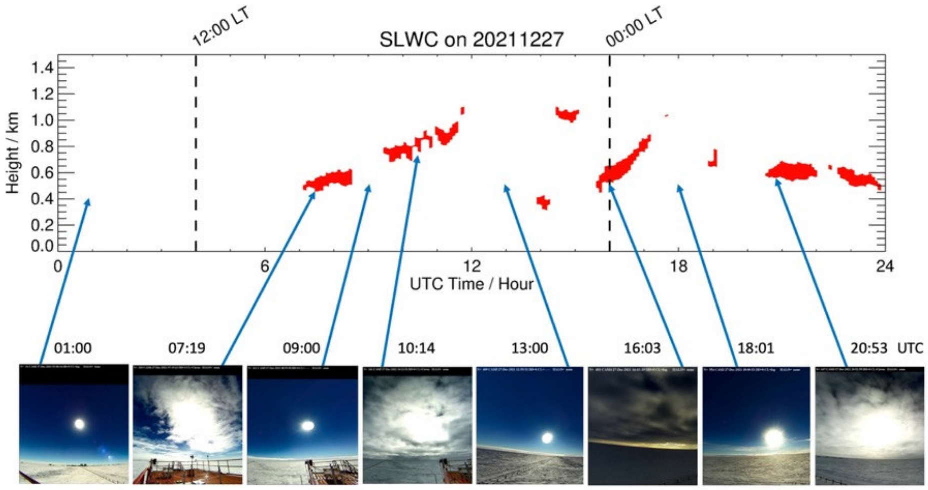

Figure 2: (Top) Time evolution (UTC, hour) of the SLWC (red areas) on 27 December 2021. (Bottom, from left to right) Snapshots from the HALO-CAM video camera taken on: 01:00 (no SLWC), 07:19 (SLWC), 09:00 (no SLWC), 10:14 (SLWC), 13:00 (no SLWC), 16:03 (SLWC), 18:01 (no SLWC) and 20:53 UTC (SLWC). The 00:00 and 12:00 local times (LT) are highlighted by 2 vertical dashed lines.

https://doi.org/10.5194/acp-2022-433
Preprint. Discussion started: 28 June 2022

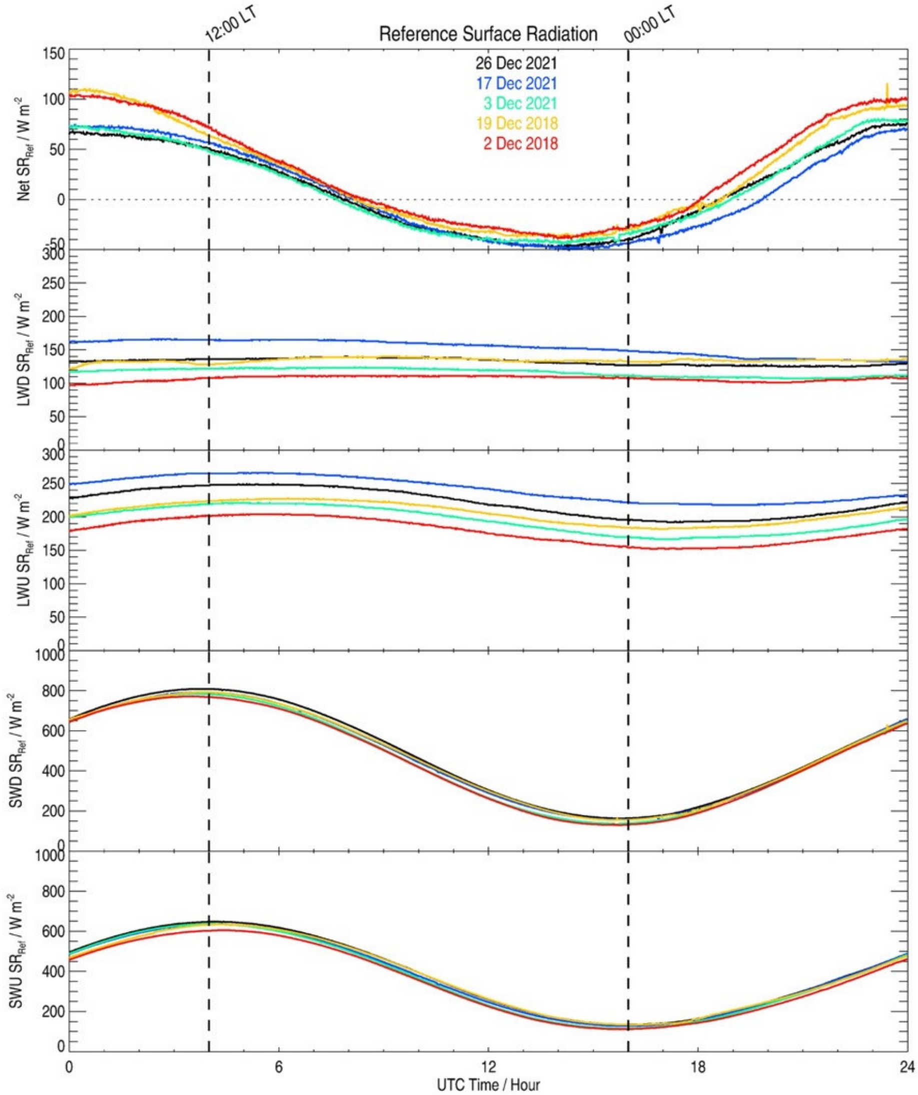

Figure 3: Time evolution (UTC, hour) of the clear-sky surface radiations (SR, W m^{-2}) observed by the BSRN instruments on 2 December 2018 (red), 19 December 2018 (orange), 3 December 2021 (green), 17 December 2021 (blue) and 26 December 2021 (black): (from top to bottom) Net SR, Longwave Downward SR (LWD SR), Longwave Upward SR (LWU SR), Shortwave Downward SR (SWD SR) and Shortwave Upward SR (SWU SR). The 00:00 and 12:00 local times (LT) are highlighted by 2 vertical dashed lines.

Atmospheric Chemistry and Physics
Discussions

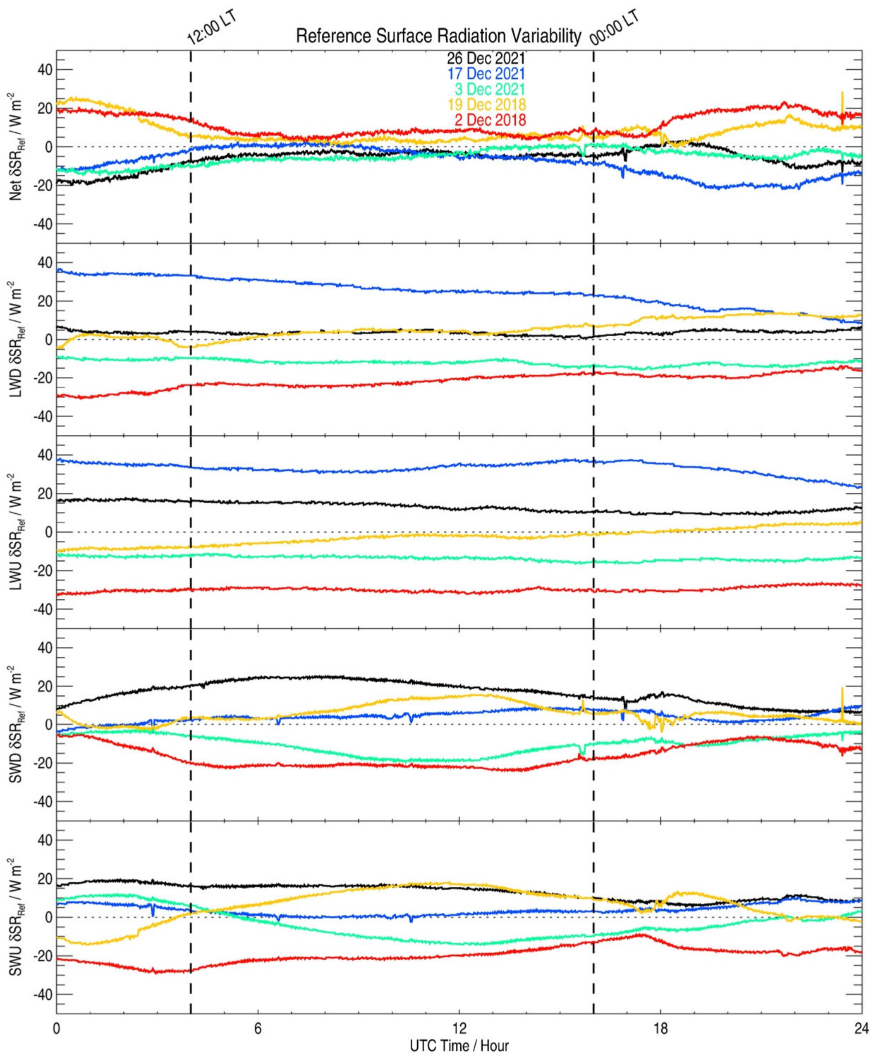

648

649 **Figure 4:** Time evolution (UTC, hour) of the clear-sky surface radiation variability (δSR_{Ref}, W

650 m^{-2}), namely the clear-sky surface radiations observed by the BSRN instruments on 2 December

651 2018 (red), 19 December 2018 (orange), 3 December 2021 (green), 17 December 2021 (blue)

652 and 26 December 2021 (black) minus the corresponding values averaged over the 5 cloud-free

653 days: (from top to bottom) Net SR, Longwave Downward SR (LWD SR), Longwave Upward

https://doi.org/10.5194/acp-2022-433
Preprint. Discussion started: 28 June 2022

SR (LWU SR), Shortwave Downward SR (SWD SR) and Shortwave Upward SR (SWU SR). The 00:00 and 12:00 local times (LT) are highlighted by 2 vertical dashed lines.

https://doi.org/10.5194/acp-2022-433
Preprint. Discussion started: 28 June 2022

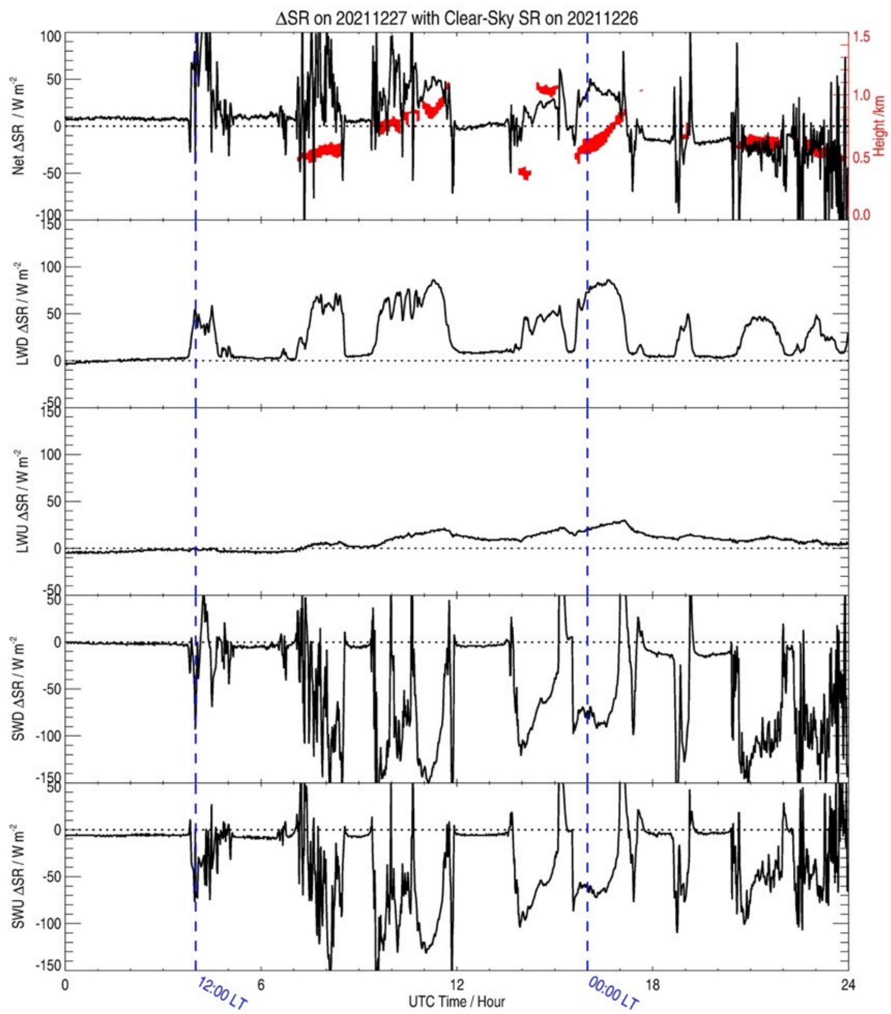

Figure 5: Time evolution (UTC, hour) of the Surface Radiation Anomaly (ΔSR), difference between the SR (W m^{-2}) measured on 27 December 2021 and the reference clear-sky (SR_{Ref}) SR (W m^{-2}) measured on 26 December 2021: (from top to bottom) Net (Net ΔSR), longwave downward (LWD ΔSR), longwave upward (LWU ΔSR), shortwave downward (SWD ΔSR) and shortwave upward (SWU ΔSR). The time evolution of the SLW cloud is highlighted by a red area in the uppermost panel, with the height on the y-axis shown on the right. The 00:00 and 12:00 local times (LT) are highlighted by 2 vertical blue dashed lines.

https://doi.org/10.5194/acp-2022-433
Preprint. Discussion started: 28 June 2022

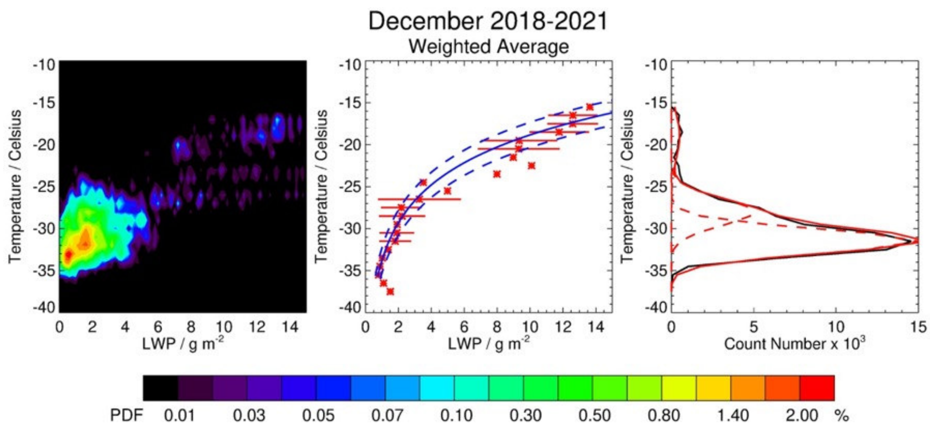

666

667 **Figure 6:** (Left) Probability Density Function (PDF, %) of the Temperature (°C) as a function
668 of Liquid Water Path (LWP, g m^{-2}) contained in the Supercooled Liquid Water clouds (SLWCs)
669 above Dome C in December 2018-2021. The PDF is defined in the text. (Centre) Weighted-
670 average LWP vs. temperature with a fitted logarithmic function (blue solid) encompassing the
671 significant points (2 dashed blue lines). Horizontal bars represent 1-sigma variability in LWP
672 per 1°C-wide bin over significant points. (Right) Temperature as a function of count number
673 per 1°C-wide bin (black solid line) with 3 fitted Gaussian functions (red dashed curves). The
674 sum of the 3 Gaussian functions is represented by a red solid line.

675

676

https://doi.org/10.5194/acp-2022-433
Preprint. Discussion started: 28 June 2022

Atmospheric Chemistry and Physics
Discussions

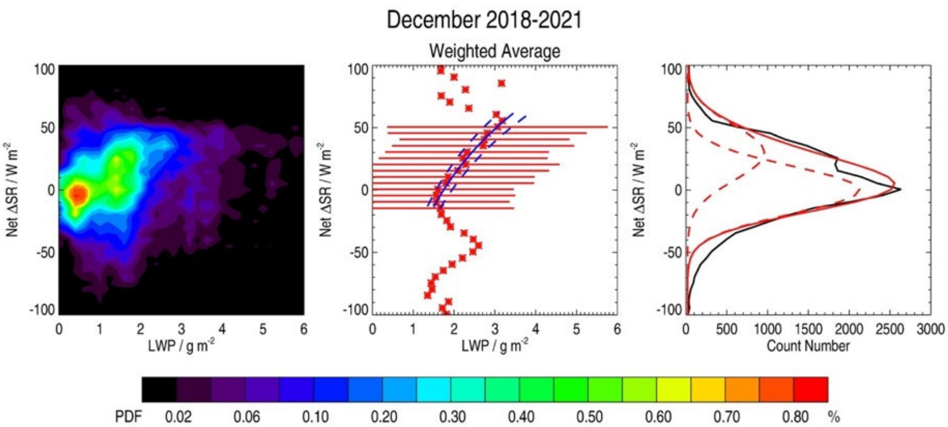

Figure 7: (Left) Probability Density Function (PDF, %) of the Net Surface Radiation Anomaly (Net ΔSR, W m^{-2}) as a function of Liquid Water Path (LWP, g m^{-2}) contained in the Supercooled Liquid Water clouds (SLWCs) above Dome C in December 2018-2021. The PDF is defined in the text. (Centre) Weighted-average LWP vs. Net ΔSR with a fitted logarithmic function (blue solid) encompassing the significant points (2 dashed blue lines). Horizontal bars represent 1-sigma variability in LWP per 5 W m^{-2}-wide bin over significant points. (Right) Net ΔSR as a function of count number per 5 W m^{-2}-wide bin (black solid line) with 2 fitted Gaussian functions (red dashed curves). The sum of the 2 Gaussian functions is represented by a red solid line.

https://doi.org/10.5194/acp-2022-433
Preprint. Discussion started: 28 June 2022

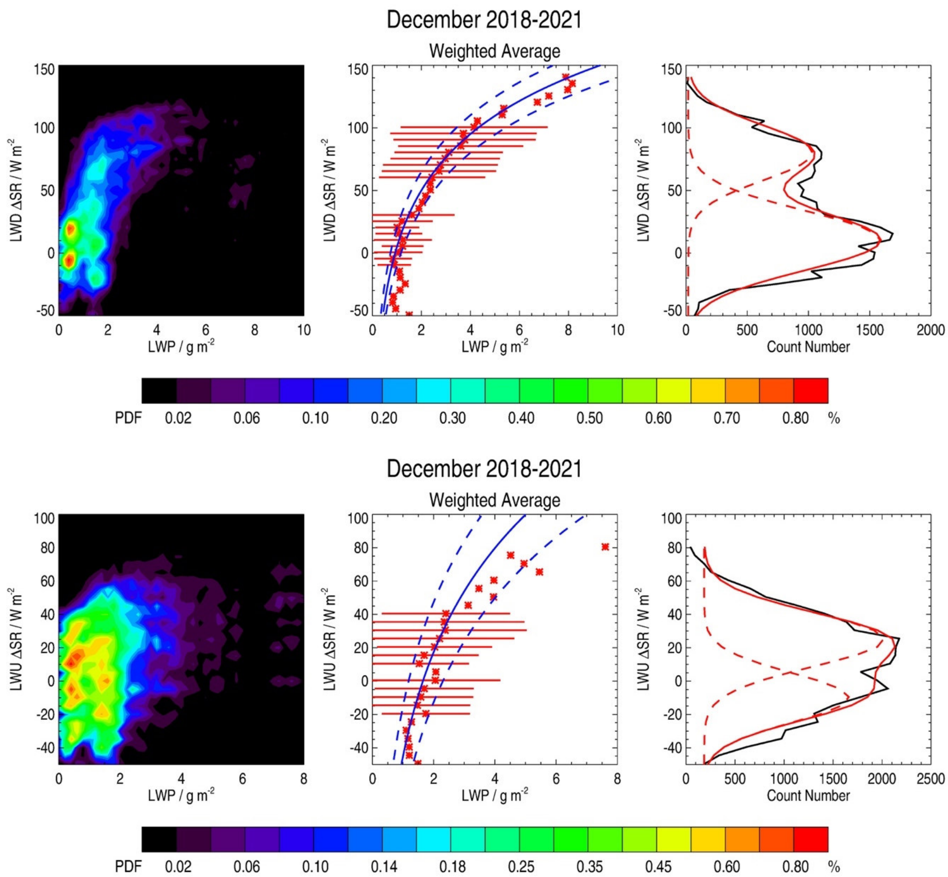

Figure 8: As in Figure 7 but for the Longwave Downward (top) and Upward (bottom) Surface Radiation Anomaly (LWD and LWU ΔSR, respectively).

https://doi.org/10.5194/acp-2022-433
Preprint. Discussion started: 28 June 2022

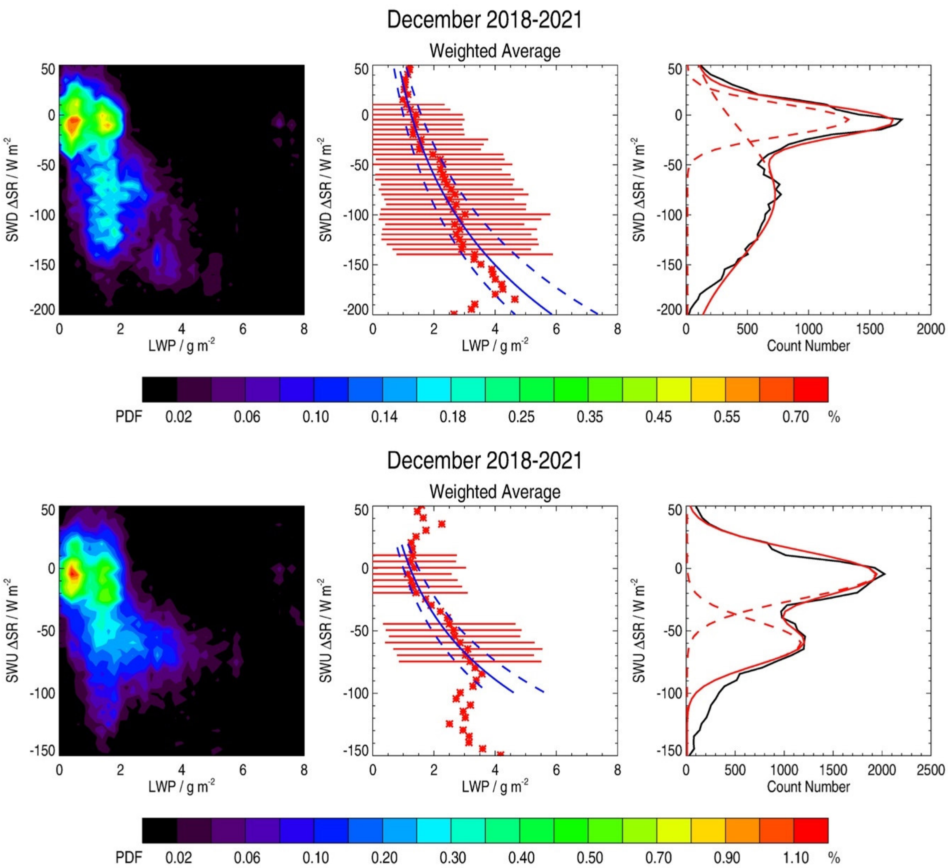

Figure 9: As in Figure 7 but for the Shortwave Downward (top) and Upward (bottom) Surface Radiation Anomaly (SWD and SWU ΔSR, respectively).